

Growth rates of coastal phytoplankton from time-series measurements with a submersible flow cytometer

Heidi M. Sosik,¹ Robert J. Olson, Michael G. Neubert, and Alexi Shalapyonok

Biology Department, Woods Hole Oceanographic Institution, Woods Hole, Massachusetts 02543

Andrew R. Solow

Marine Policy Center, Woods Hole Oceanographic Institution, Woods Hole, Massachusetts 02543

Abstract

Our understanding of the dynamics of phytoplankton communities has been limited by the space and timescales associated with traditional monitoring approaches. To overcome some of these limitations, we have developed a submersible flow cytometer (FlowCytobot) that is designed for extended autonomous monitoring of phytoplankton abundance, cell size, and pigmentation. FlowCytobot was moored on the seafloor from late July to October 2001 at the Long-term Environmental Observatory study site off the coast of New Jersey, and water samples from 5 m depth were pumped continuously through the instrument. Analysis of cells' optical properties revealed distinct populations of *Synechococcus* and cryptophytes, as well as an assemblage of other pico- and nanophytoplankton of mixed taxonomy. For each of these groups, dramatic variations in cell concentration were observed within the sampling period. Diel variations in cell scattering, which are indicative of changes in cell size, were consistent with patterns of cell growth during the light period and cell division late in the day. We developed a size-structured matrix population model that accommodates simultaneous growth and division and then used the model and size distribution data from FlowCytobot to estimate daily specific growth rates for *Synechococcus*; these estimates are independent of cell concentration and do not include mortality. The results show that a dramatic autumn decline in the concentration of *Synechococcus* can be attributed to a decrease in the specific growth rate rather than to effects of physical transport processes or trophic interactions.

The distributions of marine phytoplankton are highly variable in space and time. Evidence for this fact has come from a variety of sampling approaches, ranging from shipboard- or mooring-based measurement of in vivo chlorophyll fluorescence to satellite-based assessment of ocean color (e.g., Dickey 1991, 2001). Nevertheless, our knowledge of the factors regulating phytoplankton populations at and below the mesoscale remains limited by inadequate sampling and our inability to measure the species composition, size distribution, and growth rate of the phytoplankton community. Recently developed automated flow cytometers (Dubelaar et al. 1999; Olson et al. 2003) and cell imaging systems (Sieracki et al. 1998) are aimed at resolving some of these limitations. With these instruments, we can continuously monitor the phytoplankton at the individual cell level and document changes in the taxonomic and size structure of the phytoplankton community at a wider range of scales than has been possible with traditional techniques.

Time-series measurements of individual phytoplankton cells by conventional laboratory-based flow cytometry have provided insights into the dynamics of natural phytoplankton assemblages (Olson et al. 1990; Campbell et al. 1997; Jacques et al. 1998; DuRand et al. 2001; Li and Dickie 2001). Until now, however, cytometric approaches have been limited because they demand intensive sampling and laboratory analyses. In the present article, we report the use of our automated submersible flow cytometer ("FlowCytobot") to acquire a 2-month time series of phytoplankton properties with hourly resolution at the Long-term Environmental Observatory (LEO-15) off New Jersey, during summer and autumn 2001 (Olson et al. 2003). This site is physically complex, with tidal influence, periods of wind-driven upwelling, and variable surface and subsurface current patterns (Schofield et al. 2002). In general, the area is biologically productive but susceptible to disturbances associated with hypoxic zones that develop after strong upwelling events. Despite the important role of primary production in the development of the ecological response to these situations, relatively little is known about the abundance and composition of the phytoplankton near LEO-15 or about the combination of biological and physical factors that regulate changes in their biomass and growth rates.

Conventional laboratory-based flow cytometry has also been used to assess the growth rates of particular phytoplankton groups. From only cell abundance measurements, André et al. (1999) estimated growth and grazing rates for three groups of picophytoplankton at a station in the Equatorial Pacific. This approach is unlikely to work well, however, in physically dynamic environments, where advection

¹ Corresponding author (hsosik@whoi.edu).

Acknowledgments

We are indebted to T. Hurst and G. McDonald for excellent engineering support. O. Schofield and S. Glenn provided LEO-15 environmental data and insightful discussions, R. Petrecca assisted with FlowCytobot deployment logistics, and Y. Zhang was instrumental in facilitating access to LEO-15 environmental data.

We acknowledge the support of the National Science Foundation, the Office of Naval Research, and the National Oceanic and Atmospheric Administration's National Undersea Research Program in making this research possible.

This is Woods Hole Oceanographic Institution contribution 10733.

and spatial patchiness in abundance are expected to be large. Another approach, used by Vaultot et al. (1995) to estimate growth rates of *Prochlorococcus* in the Equatorial Pacific, combined flow cytometry with staining procedures designed to elucidate DNA content. This approach was used in subsequent studies (e.g., Binder et al. 1996; Jacquet et al. 1998; Vaultot and Marie 1999), but, because of the complex and laborious sample handling required for DNA measurements, it is not practical at present for automated sampling.

An approach for estimating growth rates that avoids some of the problems associated with spatial patchiness and sample handling is based on the interpretation of diel changes in cell size as indicative of cell growth and division, which are independent of small-scale variations in cell abundance. For example, DuRand (1995) estimated growth rates for pico- and ultraphytoplankton by assuming that increases in mean cell diameter during the day reflect cell growth. In the present article, we develop a more advanced version of this approach that uses (1) automated submersible flow cytometry to measure diel changes in cell size distribution, (2) the full size distribution (rather than a single statistic such as mean size), and (3) a matrix population model that accommodates simultaneous cell growth and division.

We used our approach to describe the temporal evolution of abundance and growth rates of *Synechococcus* at the LEO-15 site during summer–autumn 2001, as observed with FlowCytobot. The time series reflects a combination of complex, interacting processes that include changes in abundance that appear to be directly associated with the advection of water masses containing different biomass levels and other changes that appear to be driven by shifts in population-level growth rates.

FlowCytobot at LEO-15

Design and deployment—We deployed FlowCytobot (Fig. 1) on the ocean bottom at LEO-15 (“Node B,” 39°27.41’N, 74°14.75’W; Glenn et al. 2000), located 9 km off Tuckerton, New Jersey, from late July to mid-October 2001. FlowCytobot was connected by divers to a permanent underwater node at LEO-15 (in 15 m of water), which provided power from shore and allowed real-time data transmission to a shore-based computer and user-initiated communication to change instrument status. Samples from 5 m depth were analyzed continuously, except for brief interruptions associated with data transmission problems and with scheduled communication events from the shore-based computer, which was remotely operated via the Internet.

The FlowCytobot design and performance are described in detail elsewhere (Olson et al. 2003). In brief, the instrument is based on a 532-nm solid-state laser for excitation, combined with photomultiplier detectors for light scattering (forward and side) and fluorescence (575 and 680 nm). A programmable distribution-valve system selects between ambient seawater and reservoirs that contain solutions for cleaning or standard microsphere suspensions for calibration. The laser beam can be steered by remote control to allow alignment in situ, and sheath seawater (containing sodium azide to control biofouling) is filtered and recirculated during

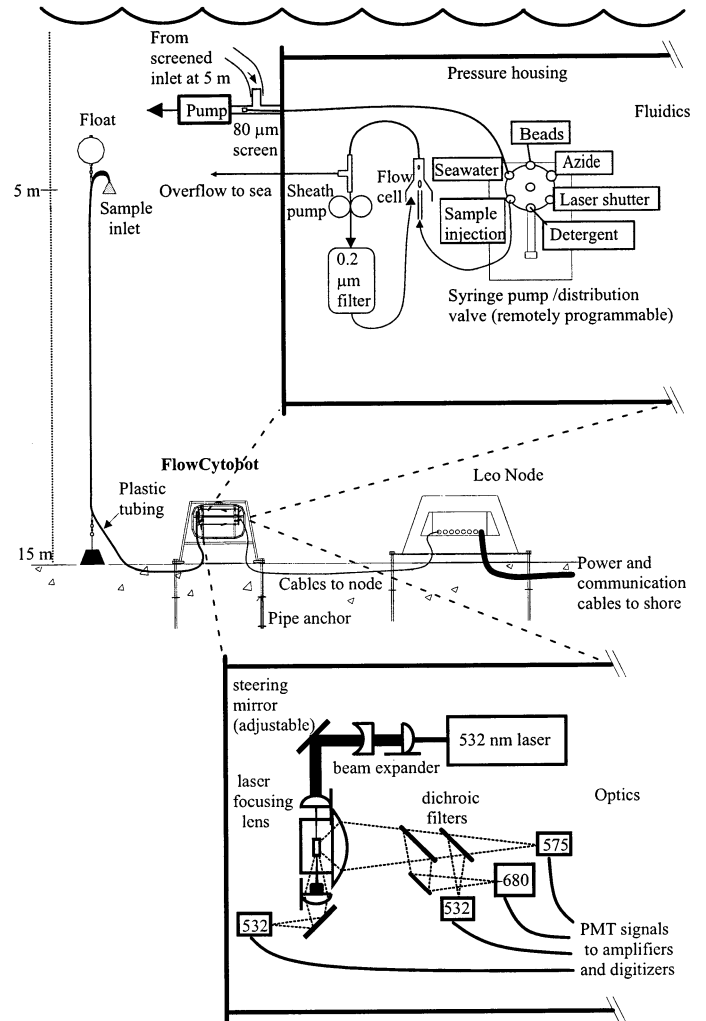


Fig. 1. FlowCytobot deployment, with schema of fluidics and optics (insets).

operation. The underwater system includes signal-processing electronics (with pairs of linear amplifiers operating at different gains to improve the instrument’s dynamic range) and a computer for sample control and data acquisition.

A variety of space- and time-resolved physical, optical, and biological properties have been measured at the LEO-15 site during focused studies, but sampling was limited during our FlowCytobot deployment. A semicontinuous record of bottom-water physical properties and shore-based meteorologic measurements is available. Bottom-water temperature, salinity, and pressure measurements were made at Node B and also at Node A, which is located 1.5 km closer to shore (39°27.70’N, 74°15.73’W, ~13 m water depth). Because there were periods of missing data in the Node B records for July–October 2001, we also used data from Node A, which filled the gaps, with substantial overlap for comparison. In addition to the underwater data, we also used surface short-wave radiation (Eppley Precision pyranometer, 0.3–3 µm) and wind data measured from a meteorologic tower at the Tuckerton Marine Station (39°30.6’N, 74°19.45’W, ~9 km from Node B) and sea-surface temper-

ature (SST) data derived from Advanced Very High Resolution Radiometer satellite imagery. These environmental data are all available online (Glenn and Schofield 2002).

Data processing—For data processing and analysis, we subdivided the record of light scattering and fluorescence signals into 1-h intervals. The appropriate light scattering and fluorescence signals for each cell were selected automatically from the instrument's two gain levels. For each 1-h interval, we then used a sequence of automated steps to classify particles into one of several groups on the basis of signal characteristics. All classification schemes used logarithmically scaled signals. We initially separated *Synechococcus* and cryptophyte phytoplankton from all other particles on the basis of their characteristic orange fluorescence from the accessory pigment phycoerythrin (Olson et al. 1990). We used a fixed threshold (in this case, the detection limit) for orange fluorescence. Consistently and objectively separating cryptophytes from *Synechococcus* was quite difficult, because the cryptophytes were always much less abundant and did not always form a distinct cluster. We used an approach that was specific for our data but was general enough to apply across the entire time series. The approach was based on side scattering and orange fluorescence signals and a combination of thresholds and a simple gradient-based search to estimate the lower boundaries of the cryptophyte cluster, the center of which was presumed to be located above the center for *Synechococcus*. This procedure generated a two-dimensional histogram and searched the region above specified scattering and fluorescence thresholds for the first minimum in the density of observations across both dimensions (i.e., a "valley" in the histogram). All signals above this boundary were assumed to be cryptophytes. Subsequently, we established the final upper boundaries of the *Synechococcus* as a threshold Mahalanobis distance from the remaining cluster centroid on chlorophyll fluorescence and side scattering. This final step was necessary to eliminate a few outlying signals with orange fluorescence that may correspond to detrital particles or green-fluorescing heterotrophs.

A suspension of standard microspheres was pumped through the flow cell approximately once per day. To identify single microspheres (apart from doublets and other particles in the microsphere suspension) in the data collected during these periods, we first located the mode signal size on each parameter independently and then included only particles whose signal sizes were within 50% of each mode. To control for changes in FlowCytobot sensitivity, all signals from phytoplankton were normalized to the mode signal size for the microspheres analyzed nearest in time.

Phytoplankton concentrations (in cells ml⁻¹) were based on the total number of cells measured and the volume of seawater analyzed, with seawater volume estimated from the pumping rate and time spent acquiring data during each hour of sampling. The data acquisition time was determined by subtracting time spent transferring data and performing other activities, such as antifouling treatment and microsphere analysis. Typical FlowCytobot sample rates during data acquisition were 50–150 samples s⁻¹, with a maximum of ~350 s⁻¹.

We estimated the volume of each phytoplankton cell with an empirical relationship between cell volume and side light scattering determined for a variety of phytoplankton species. Eleven monospecific cultures of phytoplankton (diameter, ~1–10 μm) were grown in the laboratory and analyzed with a Coulter Multisizer and with FlowCytobot. A power-law function explained 99% of the variance between cell volume and side light scattering (Olson et al. 2003). All data analysis was carried out using the MATLAB software package (MathWorks).

Time series of environmental properties—During the period of FlowCytobot deployment, environmental conditions at the study site were highly variable. There were regular oscillations in bottom pressure that were associated with tidal processes, whereas variability in bottom-water temperature and salinity appeared to occur at different scales and was irregular (Fig. 2). The largest changes in bottom-water temperature were accompanied by inverse changes in salinity, so that periods of warmer, fresher water alternated with periods of cold, saltier conditions. When bottom waters were warmest (~21–23°C), the temperatures were similar to SST values, suggesting that the water column was mixed. Daily integrated incident solar radiation varied according to cloud cover, with a modest decrease in average values indicative of the expected seasonal decline beginning in the last days of September.

Time series of Synechococcus properties—With respect to the phytoplankton, our analysis here is focused on the time-series observations for *Synechococcus*, a ubiquitous and abundant contributor to marine plankton communities (Waterbury et al. 1979; Olson et al. 1990). *Synechococcus* can be distinguished from other taxonomic groups in FlowCytobot data. During the 2-month sampling period, we observed substantial changes in the concentration of *Synechococcus* (Fig. 2E). For example, cell concentrations were as high as 5×10^5 cells ml⁻¹ during the first few days of August 2001, and then, over ~10 days, they dropped to $<1 \times 10^5$ cells ml⁻¹. Even during this period of overall decline, however, there were many large fluctuations in cell concentrations. These general features were also evident for other cell types, although the details of the high-frequency variations were often different (Olson et al. 2003).

Unraveling the underlying causes of concentration changes such as these for *Synechococcus* is complicated, because of the interrelated physiological, ecological, and physical processes that influence plankton concentration (e.g., Platt and Denman 1975; Steele 1978). On the biological side, phytoplankton cell division is offset by mortality due to trophic interactions such as grazing and viral lysis. If physical conditions are stable, the phasing of many phytoplankton growth processes to the daily light-dark cycle (Chisholm 1981; Prézélin 1992) may allow cell division and grazing rates to be estimated from diel cell concentration changes (André et al. 1999). Stability is the exception, however, especially in coastal waters, where physical processes are often the dominant source of variability in phytoplankton biomass (Platt 1972; Denman and Abbott 1994). As is evident in the water property data (Fig. 2A–C), physical variability at our sam-

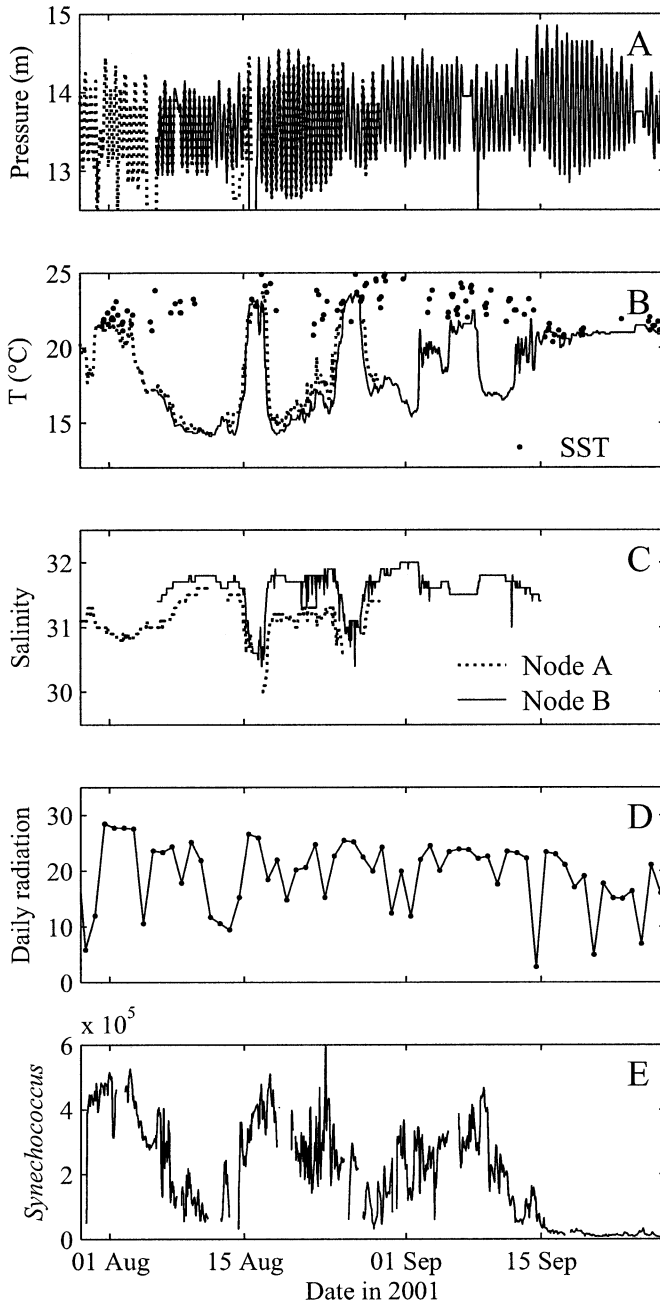


Fig. 2. Time series of measured properties during FlowCytobot deployment at the Long-term Environmental Observatory (LEO-15) site off the New Jersey coast. (A) Water pressure, (B) temperature, and (C) salinity were measured on the ocean bottom at LEO-15 Nodes "A" and "B," which are separated by 1.5 km. Satellite-derived sea-surface temperature (SST) is also shown in panel B. (D) Daily short-wave solar radiation ($\text{MJ m}^{-2} \text{d}^{-1}$) was measured 10 m above the sea surface. (E) *Synechococcus* concentrations (cells ml^{-1}) were determined for water from 5 m below the surface. To facilitate comparison with the Node B time series, the bottom pressure at Node A is displayed with a 2.8-m offset. The legend in panel C also applies to panels A and B.

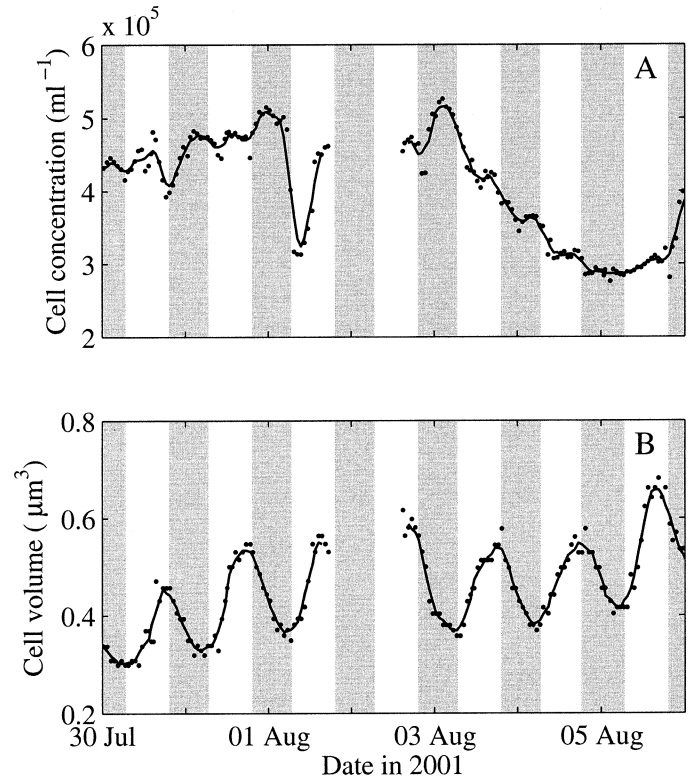


Fig. 3. *Synechococcus* properties for a 1-week subset of the time series shown in Fig. 2. Shaded bars indicate nighttime, and solid lines are four-point running means. Regular diel variations are not apparent in (A) cell concentration but are pronounced in (B) mode cell volume.

pling site was intense, to the point that regular diel variations in cell concentration were not evident (Fig. 3A), and preliminary spectral analysis did not reveal a diel variance peak in *Synechococcus* concentration.

In addition to cell concentration, FlowCytobot measurements also provide information about phytoplankton properties such as cell size. Cell size, in particular, is influenced by patterns of cell growth and division and, in contrast to cell concentration, distinct diel patterns of variation were evident in cell volume for the *Synechococcus* population. The mode cell volume generally increased during the day and decreased at night (Fig. 3B). Full size distributions for the *Synechococcus* population exhibited changes in both mode location and the shape of the distributions (Fig. 4). If changes in population size distributions can be related quantitatively to cell growth and division, then this information could be used to separate the effects of cell division from other processes (such as grazing and advection) that drive changes in cell concentration observed at a fixed location.

Determination of growth rates

Model development—For a phytoplankton population, the relative increase in mean cell volume between dawn and dusk represents a minimum estimate of the number of cell divisions per day. This approach has been used for open-ocean *Synechococcus* and other phytoplankton groups

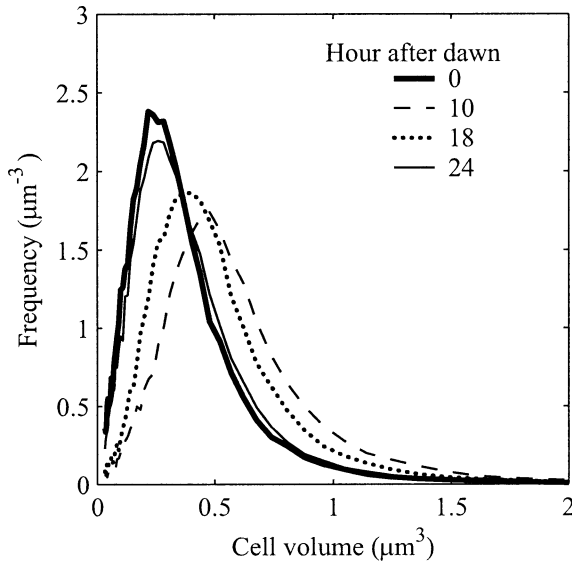


Fig. 4. Observed *Synechococcus* size distributions for several 1-h intervals on 31 July 2001. These examples, which have been normalized to the same total number of cells, show typical diel variations in mode and shape of the distributions.

(DuRand 1995; Binder et al. 1996; Vaulot and Marie 1999). The major limitation of this simple approach is that it assumes that cell growth and division are segregated during the daily cycle. Laboratory studies of *Synechococcus*, in particular, have demonstrated that growth and division can occur simultaneously in a population (Waterbury et al. 1986; Binder and Chisholm 1995; Jacquet et al. 2001), so that the simple approach underestimates growth rate. To overcome this limitation, we used a matrix population model (Caswell 2001) that incorporates the full size distribution of the population and accommodates simultaneous growth and division (Fig. 5).

We divided the population into m size classes and used $w_i(t)$ for the fraction of cells at time t that have volume between v_i and v_{i+1} . The divisions between size classes start at v_{\min} and are logarithmically spaced such that

$$v_i = v_{\min} 2^{(i-1)\Delta_v}, \quad \text{for } i = 1, \dots, m \quad (1)$$

where Δ_v is a constant. For mathematical convenience, we grouped the $w_i(t)$ into a column vector $\mathbf{w}(t)$. We projected the size distribution from time t to time $t + dt$ via matrix multiplication

$$\mathbf{w}(t + dt) = \frac{\mathbf{A}(t)\mathbf{w}(t)}{\sum_{i=1}^m \sum_{j=1}^m a_{ij}(t)w_j(t)} \quad (2)$$

where the elements of the matrix \mathbf{A} (described in the next section) are denoted a_{ij} . The denominator in Eq. 2 rescales the projection by its sum to give proportions. Defining

$$\begin{aligned} \mathbf{B}(t) &\equiv \prod_{i=0}^{(1/dt)-1} \mathbf{A}(t + idt) \\ &= \mathbf{A}(t + 1 - dt) \cdots \mathbf{A}(t + dt)\mathbf{A}(t) \end{aligned} \quad (3)$$

we projected from time t to time $t + 1$ using

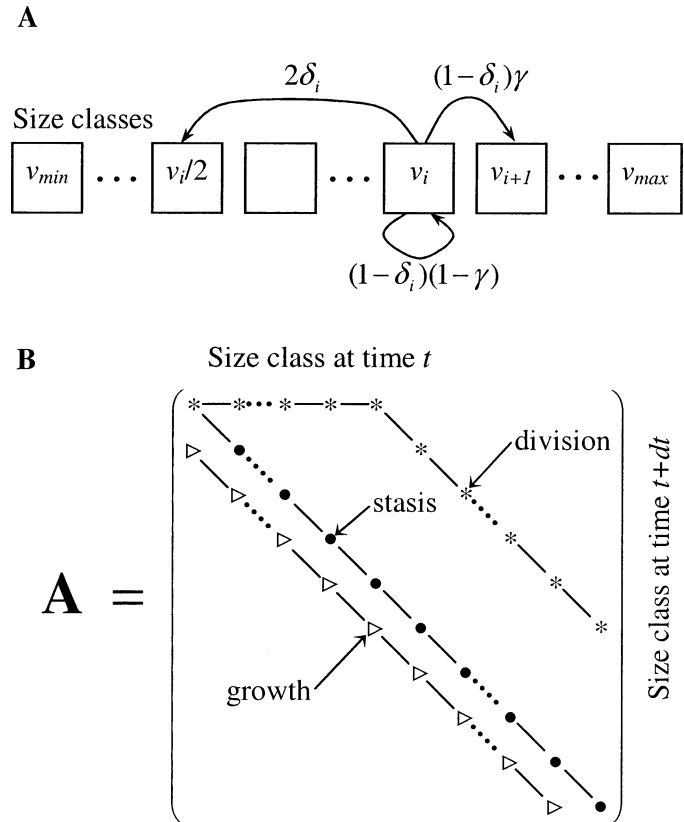


Fig. 5. Schematic representation of (A) cell size transitions occurring in one time step of the matrix population model for *Synechococcus* and (B) for the single time step projection matrix described by Eqs. 7–11. For clarity in panel A, transitions are indicated only for the size class labeled v_i . All other size classes undergo the same transitions, with the exceptions that $\gamma = 0$ for cells of size v_{\max} and cells of size v_{\min} do not change class when they divide. The structure of the upper left corner of the matrix \mathbf{A} is shown in panel B. See text for details.

$$\mathbf{w}(t + 1) = \frac{\mathbf{B}(t)\mathbf{w}(t)}{\sum_{i=1}^m \sum_{j=1}^m b_{ij}(t)w_j(t)} \quad (4)$$

(Note that the reciprocal of dt must be an integer and that the order of multiplication in Eq. 3 must be exactly as specified.) Finally, we calculated a daily specific growth rate, μ , via

$$\mu = \ln \sum_{i=1}^m u_i \quad (5)$$

where

$$\mathbf{u} = \left[\prod_{t=0}^{23} \mathbf{B}(t) \right] \mathbf{w}(0) \quad (6)$$

The elements $a_{ij}(t)$ of the projection matrix $\mathbf{A}(t)$ give the fraction of cells in size class j at time t that become cells in size class i at time $t + dt$. They represent three transitions: growth, reproduction, and stasis. In generating $\mathbf{A}(t)$, we assumed intrinsic cell death to be negligible.

The elements that account for cell growth occur along the first subdiagonal of $\mathbf{A}(t)$ and are given by

$$a_{i,i+1}(t) = \gamma(t)[1 - \delta_i(t)], \quad \text{for } i = 1, \dots, m-1 \quad (7)$$

where $\delta_i(t)$ is the fraction of cells in size class i that divide between t and $t + dt$ and $\gamma(t)$ is the fraction of cells that grow into the next size class, given that they do not divide. Later, we will describe submodels that prescribe how $\delta_i(t)$ and $\gamma(t)$ depend on cell size and environmental conditions.

Reproduction occurs via cell division, which we assumed produces two cells, each half the size of the original. If division in half would produce cells smaller than v_{\min} , we assumed that the daughter cells are both of size v_{\min} . Reproduction is thus described by elements of $\mathbf{A}(t)$ along parts of the first row

$$a_{1,i}(t) = 2\delta_i(t), \quad \text{for } i = 2, \dots, j-1 \quad (8)$$

and superdiagonal $j-1$

$$a_{i+1-j,i}(t) = 2\delta_i(t), \quad \text{for } i = j, \dots, m \quad (9)$$

where

$$j = 1 + \frac{1}{\Delta_v} \quad (10)$$

Note that Δ_v must be chosen so that j is an integer.

In one time step, a cell might not divide or grow fast enough to reach the next size class. Such cells remain in the same size class for that time step. We captured this possibility (stasis) with elements along the main diagonal of $\mathbf{A}(t)$:

$$a_{i,i}(t) = \begin{cases} [1 - \gamma(t)][1 - \delta_i(t)] + 2\delta_i(t), & \text{for } i = 1 \\ [1 - \gamma(t)][1 - \delta_i(t)], & \text{for } 2 \leq i \leq m-1 \\ [1 - \delta_i(t)], & \text{for } i = m \end{cases} \quad (11)$$

All elements of $\mathbf{A}(t)$ that were not assigned by Eqs. 7–11 were set to 0.

We assumed the maximum fraction of cells that can divide each time step to be δ_{\max} and δ_{\max} to be independent of cell size. Furthermore, we assumed that division does not occur until t_δ hours after dawn (with dawn set as $t = 0$). After hour t_δ , we assumed that the odds of division for a cell in size class i would increase as a power of cell volume (v_i):

$$\frac{\delta_i(t)}{\delta_{\max} - \delta_i(t)} = \begin{cases} 0, & \text{for } 0 \leq t < t_\delta \\ (av_i)^b, & \text{for } t_\delta \leq t < 24 \end{cases} \quad (12)$$

Rearranging Eq. 12 gives

$$\delta_i(t) = \begin{cases} 0, & \text{for } 0 \leq t < t_\delta \\ \frac{(av_i)^b}{1 + (av_i)^b} \delta_{\max}, & \text{for } t_\delta \leq t < 24 \end{cases} \quad (13)$$

Equation 13 is a simple but flexible model for cell division that incorporates the biologically reasonable assumptions that the cell cycle takes a finite time to complete and that big cells are more likely to divide than small cells.

Of the cells that do not divide at time t , a fraction $\gamma(t)$ grow into the next largest size class. $\gamma(t)$ depends on the incident radiation $E(t)$ as

$$\gamma(t) = \left\{ 1 - \exp\left[\frac{E(t)}{E^*}\right] \right\} \gamma_{\max} \quad (14)$$

γ_{\max} is the maximum fraction of cells that grow each time step, and $\gamma(t) = \gamma_{\max}/2$ when $E(t) = E^* \ln(2)$.

This completes the specification of our population model. To apply the model to a specific population, both the time of dawn and the time unit must be fixed, and the parameters dt , t_δ , m , v_{\min} , and Δ_v must be selected. For our application to *Synechococcus*, we chose to measure time in hours and took dawn to be 05:30 local time. We set $\Delta_v = 0.125$ and chose $dt = 10$ min, because, for this time step, cells are unlikely to grow more than one size class. We chose $v_{\min} = 2^{-5} \mu\text{m}^3$ and $m = 57$, so that the model size classes encompassed our full measured *Synechococcus* size distributions. t_δ was set to 6 h on the basis of evidence in the literature that suggested that natural *Synechococcus* populations typically exhibit little or no division during the morning (Waterbury et al. 1986; DuRand and Olson 1996; Jacquet et al. 1998; Vaultot and Marie 1999; Sherry and Wood 2001).

Parameter estimation—To calculate the daily specific growth rate, μ , we estimated the parameters a , b , δ_{\max} , γ_{\max} , and E^* . We did this by fitting the model to hourly observations of the population size distribution, with the parameters assumed to be constant each day.

Let $\mathbf{w}(t)$ be the observed size distribution at hour t . For a given set of parameters, our model makes a prediction $\hat{\mathbf{w}}(t+1)$ of the size distribution at hour $t+1$ given our observation at hour t , following Eq. 4:

$$\hat{\mathbf{w}}(t+1) = \frac{\mathbf{B}(t)\mathbf{w}(t)}{\sum_{i=1}^m \sum_{j=1}^m b_{ij}(t)w_j(t)} \quad (15)$$

With the series of observed $[\mathbf{w}(t)]$ and projected $[\hat{\mathbf{w}}(t)]$ size distributions in hand, we chose the parameters δ_{\max} , a , b , γ_{\max} , and E^* to minimize the weighted sum of squared deviations

$$\sigma^2 = \sum_{t=1}^{24} \sum_{i=1}^m x_i(t)^2 \quad (16)$$

where

$$\mathbf{x}(t) = N(t)[\mathbf{w}(t) - \hat{\mathbf{w}}(t)] \quad (17)$$

We minimized σ^2 , subject to the following constraints: $0 < \delta_{\max} < 1$, $0 < \gamma_{\max} < 1$, $a > 0$, $b > 0$, and $10 < E^* < 500$, with E^* measured in W m^{-2} . The weights, $N(t)$, are the total number of cells measured between $t-1$ and t ; they reflect our relative confidence in the accuracy of each observed size distribution. The result of the minimization is a best-fitting, hourly projection matrix for each hour t [called $\hat{\mathbf{B}}(t)$] and an estimated growth rate $\hat{\mu}$ (computed using Eqs. 5 and 6) for the day (Fig. 6).

We estimated confidence intervals for the specific growth rates by fitting the matrix population model to 1,000 bootstrapped data sets for each day. The bootstrapped data were

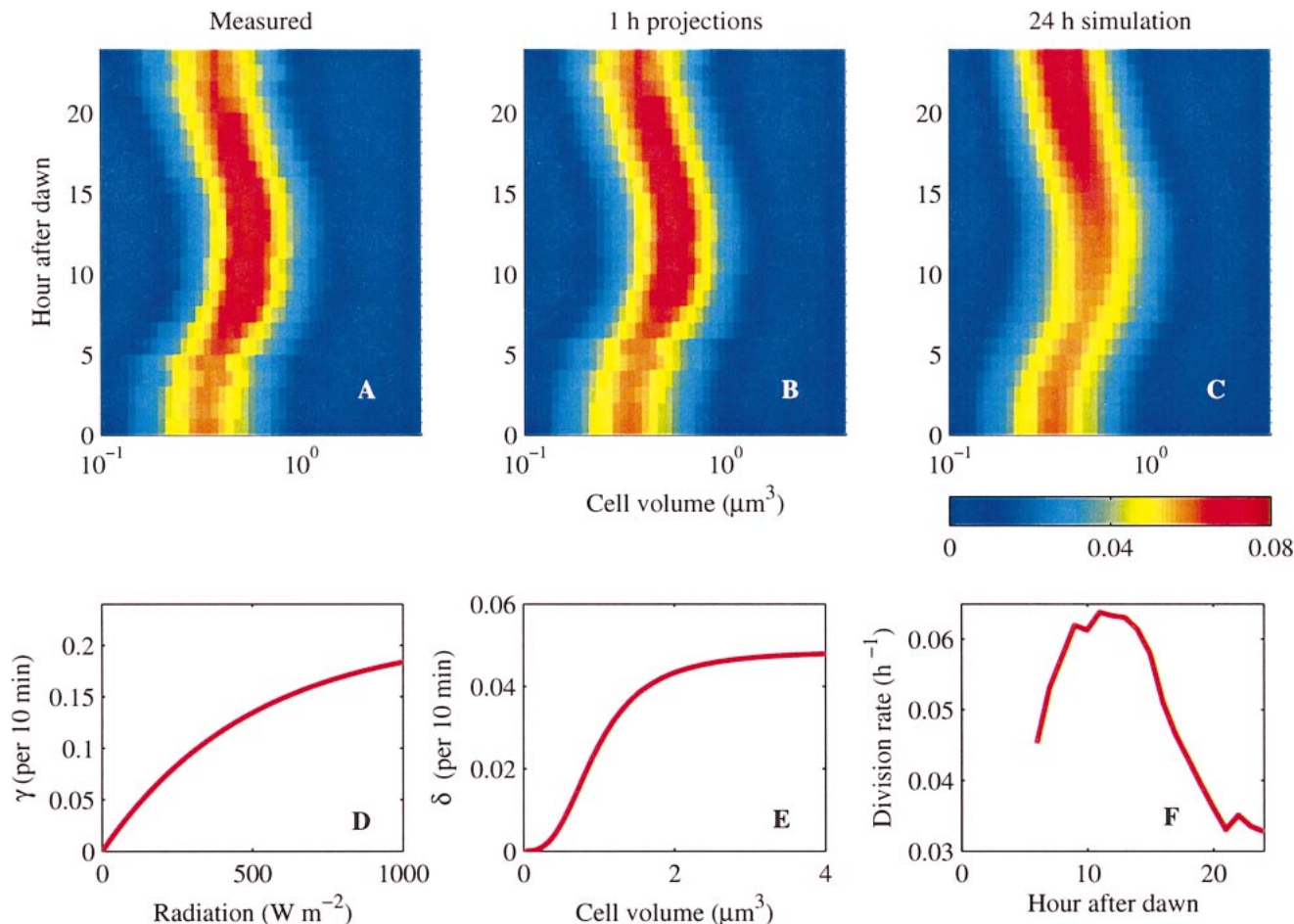


Fig. 6. (A) Measured and (B and C) modeled size distributions for *Synechococcus* in surface waters of the New Jersey shelf on 31 July 2001. Size distributions are shown for each hour of the day, with the color bar indicating relative cell concentration in logarithmically spaced size classes. The 1-h model projections in panel B were compared with the observed distributions in panel A to determine the best-fit model parameters for each day. As detailed in the text, (D) two parameters describe the light dependence of the fraction of cells progressing from one size class to the next; (E) three other parameters describe how the fraction of cells that divide depends on cell volume. (F) Calculated hourly division rates peak for several hours around dusk. Even when the model (fitted using 1-h projections) was used to project the initial size distribution forward over the entire day (C), the results were similar to the observations (A).

generated by randomly sampling with replacement from the list of measured cell volumes for each hour until the sample contained the same number of observations as in the real data. We found approximate 95% confidence intervals by omitting the top and bottom 2.5% of the growth-rate solutions.

The series of best-fitting parameters for each day of the FlowCytobot time series generated a series of γ and δ_i curves (Fig. 7). Most of the parameter values fell in relatively narrow ranges away from the constraints. There were two exceptions. First, a was usually $<1.5 \mu\text{m}^{-3}$ (83% of days), but there were a few high values ($>200 \mu\text{m}^{-3}$); on those days, δ_{max} was near 0, so δ_i remained small for all size classes. Second, the best-fitting values of E^* were often the minimum or maximum value allowed by the constraints. Relaxing the constraints had a small effect on the estimated growth rates but decreased the convergence rate of our minimization algorithm. The variability in E^* may have been due to the fact that changes in E^* reflect more than just

physiological variations in the growth response. Because we used incident solar radiation as a model input, changes in E^* also reflect changes in the subsurface light fields that cells actually experience. These light fields depend not only on incident radiation but also on attenuation in the water column and on vertical mixing. As a result, day-to-day changes in E^* are difficult to interpret.

Generally, there is little basis for evaluating our model parameter values against experimental work. We point out, however, that the hourly division rates that we estimated from the model and the measured size distributions consistently exhibited peak values during the hours around dusk (Fig. 7C), which agrees with observations of natural *Synechococcus* populations (Waterbury et al. 1986; Jacquet et al. 1998; Sherry and Wood 2001).

Time series of growth rates—By applying our model and parameter estimation approach to each day of FlowCytobot cell size data, we derived estimates of *Synechococcus*-spe-

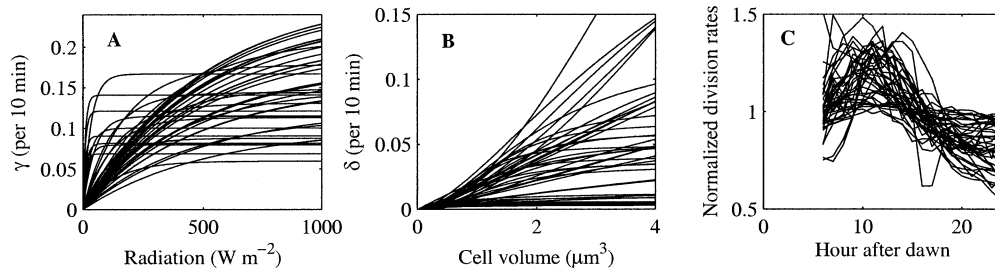


Fig. 7. (A) Growth fraction, γ , as a function of incident radiation and (B) division fraction, δ , as a function of cell volume for each day of the FlowCytobot time series as derived from the best-fitting model parameters (see text for details). Parameters fell in the following ranges: $0.06 < \gamma_{\max} < 0.26$, $10 < E^* < 500 \text{ W m}^{-2}$, $0.003 < \delta_{\max} < 0.992$, $1.2 \times 10^{-3} < a < 3.5 \times 10^4 \mu\text{m}^{-3}$, and $0.66 < b < 3.09$. (C) Hourly cell division rates normalized to the mean value for each day show that the model results predict peak values around dusk.

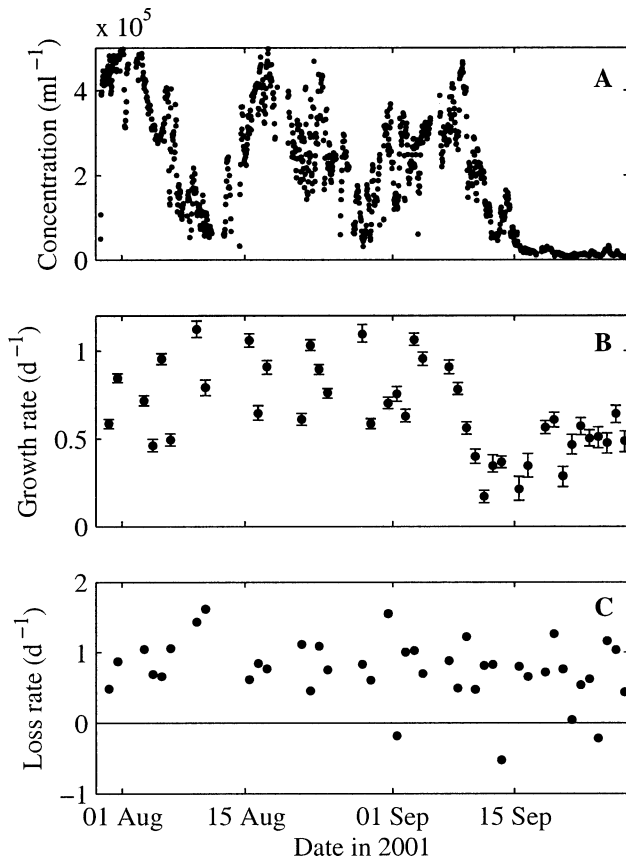


Fig. 8. Time series of *Synechococcus* population properties in surface waters of the New Jersey shelf. (A) Cell concentrations with 1-h resolution were determined directly from FlowCytobot measurements. (B) Daily specific growth rates of *Synechococcus* were determined from measured cell size distributions and a linear matrix model for cell growth and division over the diel cycle. Growth rates were estimated for 41 d that had sufficient cell size data. Error bars represent estimated 95% confidence intervals. (C) Apparent cell-specific loss rates were estimated by the difference between the specific growth rates and the observed daily rates of population increase, calculated directly from the concentrations in panel A. Grazing by microzooplankton would contribute to positive loss rates, whereas physical processes, including water mass mixing and advection, could result in positive or negative loss rates.

cific growth rate for each day of the time series (Fig. 8). Because the model was based only on changes in the shape of the cell size distribution over intervals from one dawn to the next, these specific growth rates are independent of observed changes in cell concentration. As was expected, the model-derived growth rates were correlated over the time series, with the observed dusk-to-dawn changes in mode cell light scattering for the *Synechococcus* population ($r^2 = 0.52$, not shown). Growth rates faster than one division per day (i.e., $\mu > 0.69 \text{ d}^{-1}$) were often observed during August. These high rates are consistent with reports for natural populations of *Synechococcus* from other studies (Waterbury et al. 1986; Carpenter and Campbell 1988; Jacquet et al. 1998). The most dramatic feature of the time series was a sharp drop in growth rate during the second week in September. Overall, growth rates were between 0.17 and 1.13 d^{-1} over the 2-month time series and often varied by as much as twofold from one day to the next. The bootstrap results showed that this variability cannot be explained by sampling variability alone (Fig. 8B).

From the specific growth rates and the observed changes in cell concentration, we also calculated net population loss rates. These loss rates were determined as the difference between the specific growth rate and the exponential rate of change in observed cell concentration from one dawn to the next. The rate of change in cell concentration reflects cell division plus other processes that influence cell concentration observed at a single location; thus, our loss rate estimates represent the net effect of these other processes. These processes include grazing, sinking, mixing, and advection, and their net effect can be either an increase or decrease in cell concentration. Loss rates were highly variable but were almost always positive (i.e., a net sink for cell concentration) and were usually $>0.5 \text{ d}^{-1}$.

Discussion

The observed concentration variations in any natural population can be ascribed to the net effect of reproduction, biological or ecological losses such as intrinsic mortality and predation, and immigration plus emigration. In a time series such as the one we have documented for a unicellular picoplanktonic organism, increases can occur due to cell di-

vision, and losses from ecological interactions such as grazing by microzooplankton or viral infection are probably important; in addition, the mixing and advection of water masses with different cell abundances can result in increases or decreases in the concentration observed at a single location. Because our size distribution model allowed us to determine the cell-specific growth rate of the cells, independent of observed changes in cell concentration, we were able to separate the effects of cell division from these other processes.

For time-series observations in the Equatorial Pacific, André et al. (1999) used a cell cycle-based model to determine daily growth and grazing rates from cell concentrations. For that environment, which is less physically dynamic than the LEO-15 area, diel changes in cell concentration were evident, making this approach practical. High temporal and spatial patchiness in cell concentration, which are expected for continental shelf environments, obscured regular diel variations in cell concentration in our data (Fig. 3A); a similar result was reported by Jacquet et al. (1998) for coastal Mediterranean waters. Despite these findings, our results suggest that diel variations in cell size, a property that depends strongly on cell physiology, are preserved across concentration patches. These kinds of characteristic diel variations in cell light scattering and size have been documented in a variety of open ocean (Olson et al. 1990; DuRand and Olson 1996; Vaultot and Marie 1999) and coastal (Jacquet et al. 1998) phytoplankton groups. As a consequence, estimating growth rates from size distributions is likely to have broad applicability, given the ability to measure high-resolution time series with instruments such as FlowCytobot.

From our data and model results, we have inferred that physical processes caused the observed *Synechococcus* population decline during early August 2001 on the New Jersey shelf (Fig. 7A). There is no evidence that the decline was associated with a decrease in the specific growth rate before or during this period (Fig. 7B). As a consequence, the cell-specific loss rate must have increased (Fig. 7C). Although we cannot unambiguously distinguish between biological losses, such as grazing, and losses due to the physical transport of cells, other evidence suggests that physical processes played an important role in the observed population decline. Bottom-water temperatures at LEO-15 experienced an $\sim 8^\circ\text{C}$ drop during this period (Fig. 2B), which was most likely due to the upwelling of deeper, colder shelf waters forced by the predominantly southwesterly winds. Wind-driven upwelling is common in this area and has been reported elsewhere to bring in water masses with higher chlorophyll concentrations and particle loads (Glenn et al. 2000; Schofield et al. 2002). In 2001, however, a series of upwelling events similar to the one we observed during August occurred earlier during the summer, and these earlier events were accompanied by lower turbidity at LEO-15 (O. Schofield pers. comm.), which is consistent with our observation of low phytoplankton concentration. Later in August, another apparent upwelling event occurred, but, in this case, cell concentrations did not decrease as sharply, nor did they remain low during the entire period of low bottom temperature (Fig. 2). These results underscore the complexity of predicting consequences of events like upwelling on plankton distributions and empha-

size the need for combined physical and biological time-series observations.

The largest change that we observed in the *Synechococcus* concentration occurred during mid-September (Fig. 8A). In contrast to the population decline in early August, this dramatic decline appears to have had a physiological cause. During the September decline, cell-specific loss rates did not increase, but specific growth rates decreased. Specific growth rates were high at the end of August and the beginning of September, with cells consistently dividing more than once per day (Fig. 8B). Then, over 4 d beginning on 7 September, growth rates dropped from >0.9 to <0.2 d^{-1} . Growth rates stayed well below one doubling per day (i.e., $\mu < 0.69$ d^{-1}) for the remainder of September, whereas cell concentrations fell from $>4 \times 10^5$ to $<8 \times 10^3$ ml^{-1} and never recovered (Fig. 8A). Although we do not know what caused the initial decrease in the *Synechococcus* growth rate, the persistently low rates observed after 15 September could have been caused by a combination of reduced temperature and reduced light available for photosynthesis. As was expected for the season, SST and incident irradiance were lower (by $\sim 2^\circ\text{C}$ and $\sim 20\%$, respectively) during the last half compared with the first half of September. The phytoplankton were probably exposed to even lower light because of deep mixing; after 15 September, bottom-water temperatures were very close to SST values, which suggests that the entire water column was well mixed. The idea that *Synechococcus* growth rates remained low because of low light exposure is also supported by the observation that cellular chlorophyll levels (inferred from cell fluorescence measurements by FlowCytobot) increased during September (they were 60% higher after 15 September), a response that is typical for phytoplankton acclimating to lower light conditions (Falkowski 1980).

The fundamental response of a plankton population to environmental change is expressed in its specific growth rate, but growth rates cannot be determined from traditional measurements of pigment biomass or even cell abundance in the dynamic coastal ocean. In these systems, we expect biological and physical variability to be linked across various space and timescales. For instance, upwelling may introduce water with low cell concentrations but with nutrients that ultimately stimulate biological processes. In addition, changes in cell growth rates, such as those that occurred during September, occur because organisms are responding to their physical environment—in this case, lower light caused by vertical mixing. Particularly because of these complexities, it is exciting to have the ability to begin separating immediate physical and biological effects on populations. Population modeling that uses data from automated submersible instrumentation for individual cell analysis now enables us to estimate growth rates and thus to distinguish physiologically driven change in phytoplankton abundance from more incidental fluctuations. With a single 2-month time series, we were able to contrast a major population change driven by coastal ocean physics with a similar change driven by biological variability. Our example focused on a single taxonomic group of phytoplankton, but the approach can be generalized to any population of cells that can be discriminated from others in an assemblage, perhaps with the aid of

taxon-specific molecular probes (Amann et al. 1990; Cooksey 1998). With future work to obtain multiyear records as part of interdisciplinary coastal ocean monitoring systems (Malone and Cole 2000), we expect this kind of investigation to help answer longstanding questions about the initiation and fate of phytoplankton blooms and the regulation of diversity in plankton.

References

- AMANN, R., B. B. BINDER, R. J. OLSON, S. W. CHISHOLM, R. DEV-EREUX, AND D. A. STAHL. 1990. Combining 16s rRNA-targeted oligonucleotide probes with flow cytometry for analyzing mixed microbial populations. *Appl. Environ. Microbiol.* **56**: 1919–1925.
- ANDRÉ, J.-M., C. NAVARETTE, J. BLANCHOT, AND M.-H. RADENAC. 1999. Picophytoplankton dynamics in the equatorial Pacific: Growth and grazing rates from cytometric counts. *J. Geophys. Res.* **104**: 3369–3380.
- BINDER, B. J., AND S. W. CHISHOLM. 1995. Cell cycle regulation in marine *Synechococcus* sp. strains. *Appl. Environ. Microbiol.* **61**: 708–717.
- , R. J. OLSON, S. L. FRANKEL, AND A. Z. WORDEN. 1996. Dynamics of picophytoplankton, ultraphytoplankton and bacteria in the Central Equatorial Pacific. *Deep-Sea Res. II* **43**: 907–931.
- CAMPBELL, L., L. HONGBIN, AND D. VAULOT. 1997. Annual variability of phytoplankton and bacteria in the subtropical North Pacific Ocean at station ALOHA during the 1991–1994 ENSO event. *Deep-Sea Res. I* **44**: 167–192.
- CARPENTER, E. J., AND L. CAMPBELL. 1988. Diel patterns of cell division and growth rates of *Synechococcus* spp. in Long Island Sound. *Mar. Ecol. Prog. Ser.* **47**: 179–183.
- CASWELL, H. 2001. Matrix population models, 2nd ed. Sinauer.
- CHISHOLM, S. W. 1981. Temporal patterns of cell division in unicellular algae, p. 150–181. *In* T. Platt [ed.], *Physiological bases of phytoplankton ecology*. *Can. Bull. Fish. Aquat. Sci.* 120.
- COOKSEY, K. E. 1998. Molecular approaches to the study of the ocean. Chapman and Hall.
- DENMAN, K. L., AND M. R. ABBOTT. 1994. Time scales of pattern evolution from cross-spectrum analysis of advanced very high resolution radiometer and coastal zone color scanner imagery. *J. Geophys. Res.* **99**: 7433–7442.
- DICKEY, T. 1991. The emergence of concurrent high-resolution physical and bio-optical measurements in the upper ocean and their applications. *Rev. Geophys.* **29**: 383–413.
- . 2001. New technologies and their roles in advancing recent biogeochemical studies. *Oceanography* **14**: 108–120.
- DUBELAAR, G. B. J., P. L. GERRITZEN, A. E. R. BEEKER, R. R. JONKER, AND K. TANGEN. 1999. Design and first results of CytoBuoy: A wireless flow cytometer for in situ analysis of marine and fresh waters. *Cytometry* **37**: 247–254.
- DURAND, M. D. 1995. Phytoplankton growth and diel variations in beam attenuation through individual cell analysis. Ph.D. thesis, Massachusetts Institute of Technology, Woods Hole Oceanographic Institution.
- , AND R. J. OLSON. 1996. Contributions of phytoplankton light scattering and cell concentration changes to diel variations in beam attenuation in the equatorial Pacific from flow cytometric measurements of pico-, ultra- and nanoplankton. *Deep-Sea Res. II* **43**: 891–906.
- , ———, AND S. W. CHISHOLM. 2001. Phytoplankton population dynamics at the Bermuda Atlantic time-series station in the Sargasso Sea. *Deep-Sea Res. II* **48**: 1983–2003.
- FALKOWSKI, P. G. 1980. Light-shade adaptation in marine phytoplankton, p. 99–119. *In* P. G. Falkowski [ed.], *Primary productivity in the sea*. Plenum.
- GLENN, S. M., W. BOICOURT, B. PARKER, AND T. D. DICKEY. 2000. Operational observation networks for ports, a large estuary and an open shelf. *Oceanography* **13**: 12–23.
- , AND O. SCHOFIELD. 2002. Rutgers University's coastal ocean observation laboratory Web site. Available at: <http://marine.rutgers.edu/mrs/>.
- JACQUET, S., J. LENNON, D. MARIE, AND D. VAULOT. 1998. Picoplankton population dynamics in coastal waters of the north-western Mediterranean Sea. *Limnol. Oceanogr.* **43**: 1916–1931.
- , F. PARTENSKY, J. LENNON, AND D. VAULOT. 2001. Diel patterns of growth and division in marine picoplankton in culture. *J. Phycol.* **37**: 357–369.
- LI, W. K. W., AND P. M. DICKIE. 2001. Monitoring phytoplankton, bacterioplankton, and virioplankton in a coastal inlet (Bedford Basin) by flow cytometry. *Cytometry* **44**: 236–246.
- MALONE, T. C., AND M. COLE. 2000. Toward a global scale coastal ocean observing system. *Oceanography* **13**: 7–11.
- OLSON, R. J., S. W. CHISHOLM, E. R. ZETTLER, AND E. V. ARMBRUST. 1990. Pigments, size, and distribution of *Synechococcus* in the North Atlantic and Pacific Oceans. *Limnol. Oceanogr.* **35**: 45–58.
- , A. A. SHALAPYONOK, AND H. M. SOSIK. 2003. An automated submersible flow cytometer for pico- and nanophytoplankton: FlowCytobot. *Deep-Sea Res. I* **50**: 301–315.
- PLATT, T. 1972. Local phytoplankton abundance and turbulence. *Deep-Sea Res.* **19**: 183–187.
- , AND K. L. DENMAN. 1975. Spectral analysis in ecology. *Annu. Rev. Ecol. Syst.* **6**: 189–210.
- PRÉZELIN, B. B. 1992. Diel periodicity in phytoplankton productivity. *Hydrobiologia* **238**: 1–35.
- SCHOFIELD, O., AND OTHERS. 2002. The Long-term Ecosystem Observatory: An integrated coastal observatory. *IEEE J. Ocean. Eng.* **27**: 193–201.
- SHERRY, N. D., AND A. M. WOOD. 2001. Phycocyanin-containing picocyanobacteria in the Arabian Sea in February 1995: Diel patterns, spatial variability, and growth rates. *Deep-Sea Res. II* **48**: 1263–1283.
- SIERACKI, C. K., M. E. SIERACKI, AND C. S. YENTSCH. 1998. An imaging-in-flow system for automated analysis of marine microplankton. *Mar. Ecol. Prog. Ser.* **168**: 285–296.
- STEELE, J. H. 1978. Spatial pattern in plankton communities. Plenum.
- VAULOT, D., AND D. MARIE. 1999. Diel variability of photosynthetic picoplankton in the equatorial Pacific. *J. Geophys. Res.* **104**: 3297–3310.
- , R. J. OLSON, AND S. W. CHISHOLM. 1995. Growth of *Prochlorococcus*, a photosynthetic prokaryote, in the equatorial Pacific Ocean. *Science* **268**: 1480–1482.
- WATERBURY, J. B., S. W. WATSON, F. W. VALOIS, AND D. G. FRANKS. 1986. Biological and ecological characterization of the marine unicellular cyanobacterium *Synechococcus*, p. 71–120. *In* T. Platt and W. K. W. Li [eds.], *Photosynthetic picoplankton*. *Can. Bull. Fish. Aquat. Sci.* 214.

Received: 27 September 2002

Accepted: 11 March 2003

Amended: 4 April 2003